Journal of Power Sources 198 (2012) 287–293

Contents lists available at SciVerse ScienceDirect

Journal of Power Sources

journal homepage: www.elsevier.com/locate/jpowsour

# Synthesis and electrochemical performance of rod-like $LiV_3O_8$ cathode materials for rechargeable lithium batteries

Y.Q. Qiao, X.L. Wang*, J.P. Zhou, J. Zhang, C.D. Gu, J.P. Tu*

*State Key Laboratory of Silicon Materials and Department of Materials Science and Engineering, Zhejiang University, Hangzhou 310027, China*

ARTICLE INFO

*Article history:*
Received 2 September 2011
Accepted 9 October 2011
Available online 13 October 2011

*Keywords:*
Lithium vanadate oxide
Rod-like morphology
Cathode material
Rechargeable lithium battery

ABSTRACT

Rod-like $LiV_3O_8$ composites have been fabricated by using a carbamide-assisted rheological phase reaction method. The electrochemical performances of the $LiV_3O_8$ materials prepared under different conditions are investigated by cyclic voltammograms, galvanostatic charge–discharge tests and electrochemical impedance spectroscopy (EIS). The rod-like $LiV_3O_8$ calcined at 500 °C has the optimal performance, delivering an initial discharge capacity of 273.6 and 250.4 mAh $g^{-1}$ between 2.0 V and 4.0 V at a current density of 50 and 120 mA $g^{-1}$, respectively. After 60 cycles by applying 50 mA $g^{-1}$, a discharge capacity of 213.0 mAh $g^{-1}$ is obtained, showing a good cycling performance. The EIS studies show that the 500 °C-$LiV_3O_8$ electrode has very low impedance increase during 1st to 240th discharge-charge cycles. All these results indicate that the rod-like $LiV_3O_8$ compound has a promising application as the cathode material for rechargeable lithium batteries.



## 1. Introduction

Rechargeable lithium ion batteries are considered as the most advanced electrochemical energy storage and transfer systems in portable devices and hybrid electric vehicles [1,2]. It is well known that the cathode materials are particularly critical in determining the performance of lithium ion batteries. Layered lithium vanadate oxide $LiV_3O_8$ has been researched extensively as a cathode material because of its high capacity, high energy density, acceptable cyclability and facile preparation [3–5]. For the sake of practical applications, many strategies have been employed to further enhance the electrochemical performance of $LiV_3O_8$ such as doping, coating and structural/morphological modification. To date, substitution of lithium/vanadium with other elements such as Ni [6], Na [7], Cu [8], Ag [9], Mo [10], Y [11], Si [12], B [13] and F [14] has been proved to be beneficial in improving the electrochemical performance of $LiV_3O_8$ in a certain extent. Many researchers have found that coating with $AlPO_4$ [15], carbon [16] and ppy [17–19] could also play a very effective role in the enhancement of electrochemical performance of the materials.

As has been reported in previous publications, another important factor influences the electrochemical properties of this compound is structural/morphological characteristic. Actually, these structural and morphological characteristics are strongly dependent on the synthesis conditions. In general, traditional solid-state reaction needs high heating temperature and long time, which has met difficulty to control the particle size and homogeneity of the final powders [20,21]. Therefore, low temperature solid-state reaction methods have been proposed to reduce the particle size and save the energy [22,23]. Recently, pray pyrolysis was used to prepare the spherical $LiV_3O_8$ coexisted with rod-like crystals and the composite exhibited good electrochemical performance [24]. Liu et al. [25] and Ma et al. [26] prepared $LiV_3O_8$ materials with porous state by two different methods, and both the compounds showed excellent electrochemical performance due to their own especial characteristics. Zhang et al. [27] demonstrated that the flaky $LiV_3O_8$ prepared by a vapor-diffusion-controlled sol–gel method delivered a reversible capacity of 250 mAh $g^{-1}$ at 0.1 C, and also exhibited good capacity retention.

In recent years, one-dimensional (1D) materials have been considered as an effective way for achieving high-rate capability and enhancing power performance because they can provide efficient one-dimensional electron transport pathways and accommodate the volume changes during charge/discharge processes [28–30]. So far, rod-like $LiV_3O_8$ compounds have been prepared by several different methods. Xu et al. [31] employed a hydrothermal reaction to synthesize $LiV_3O_8$ nanorods, and the material exhibited a reversible capacity of 302 mAh $g^{-1}$ in a wider potential range of 1.8–4.0 V at a current density of 0.3 mA $cm^{-2}$. Sakunthala et al. [32] prepared $LiV_3O_8$ rods by a surfactant-assisted polymer precursor method, a discharge capacity of 206 mAh $g^{-1}$ could

* Corresponding authors. Tel.: +86 571 87952856; fax: +86 571 87952573.
*E-mail addresses:* wangxl@zju.edu.cn (X.L. Wang), tujp@zju.edu.cn (J.P. Tu).

0378-7753/$ – see front matter © 2011 Elsevier B.V. All rights reserved.
doi:10.1016/j.jpowsour.2011.10.023

be achieved in the potential range of 2.0–4.0 V at a current density of 30 mA $g^{-1}$. Liu et al. [33] first synthesized $VO_2$ nanorods as the vanadium precursor, and then employed solid-state reaction to fabricate $LiV_3O_8$ nanorods by adding $LiOH{\cdot}H_2O$. The $LiV_3O_8$ nanorods exhibited as high as 348 mAh $g^{-1}$ initial discharge capacity at 20 mA $g^{-1}$ in a more wide potential window of 1.5–4.5 V. Caballero and co-workers [34] synthesized $LiV_3O_8$ rods by using the precursors $VO(C_5H_8O_2)_2$ and $Li(CH_3–COO)$, and carried out the material as an electrode for aqueous rechargeable lithium batteries. Recently, a low-temperature thermal co-decomposition method was used for fabricating a $LiV_3O_8$ nanorod [35], showing a particularly high discharge capacity of 320 mAh $g^{-1}$ at a current density of 100 mA $g^{-1}$ in the potential range of 1.5–4.0 V. In this present work, we described a carbamide-assisted rheological phase reaction synthesis for the preparation of rod-like $LiV_3O_8$ materials. The structure and electrochemical behaviors were investigated, presenting a good electrochemical property.

## 2. Experimental

$LiOH{\cdot}H_2O$, $NH_4VO_3$ and carbamide ($NH_2CONH_2$) were used as raw materials. In a typical synthesis, stoichiometric amounts of $LiOH{\cdot}H_2O$ and $NH_4VO_3$ with carbamide (21 wt.% of the total raw materials) were added into a polytetrafluoroethylene (PTFE) container. Then an appropriate amount of de-ionized water was added into the container and stirred for 20 min by magnetic stirring. The container was sealed and maintained at 200 °C for 6 h, and cooled to room temperature. Afterwards, the obtained precursor was dried at 70 °C, and then was calcined at 450–600 °C in air for 6 h to yield the final products.

The morphologies and structures of the as-synthesized powders were characterized using field emission scanning electron microscopy (FESEM, FEI SIRION), X-ray diffraction (XRD, Philips PC-APD with Cu Kα radiation) and high-resolution transmission electron microscopy (TEM, Tecnai G2 F30 S-Twin). The unit-cell lattice parameters were obtained by Rietveld refinement of the powder XRD data using the software Maud [36–38].

Electrochemical performances of $LiV_3O_8$ were investigated using CR2025 coin-type cell. A metallic lithium foil served as the anode. The cathode consisted of 75 wt.% active material, 15 wt.% acetylene black and 10 wt.% polyvinylidene fluoride (PVDF) on aluminum foil. 1 M $LiPF_6$ in ethylene carbonate (EC)-dimethyl carbonate (DMC) (1:1 in volume) was used as the electrolyte, and a polypropylene micro-porous film (Cellgard 2300) as the separator. The cells were assembled in an argon-filled glove box with $H_2O$ and $O_2$ concentrations below 1 ppm. The charge–discharge tests were conducted on LAND battery program-control test system (Wuhan, China) between 2.0 and 4.0 V by applying from 50 to 120 mA $g^{-1}$ current densities at room temperature. CV tests were performed on CHI660C electrochemical workstation in the potential range of 2.0–4.0 V (vs. $Li/Li^+$) at a scan rate of 0.1 mV $s^{-1}$. For EIS measurements, the test cells were with the metallic lithium foil as both the reference and counter electrodes. The EIS measurements were performed on CHI660C electrochemical workstation over a frequency range of 100 kHz to 10 mHz by applying an AC signal of 5 mV.

## 3. Results and discussion

The XRD patterns and the Rietveld refinement of the $LiV_3O_8$ powders are shown in Fig. 1. Only the main ($h\,k\,l$) lines are indexed for clarity and the refinement parameters of the powders are listed in Table 1. These refinement parameters are similar to the previous reports [27,32,34]. It can be found that the compounds synthesized in the temperature range of 450–600 °C are all composed of two phases. The main phase is $LiV_3O_8$ with layered monoclinic structure and belongs to the *P21/m* space group (JCPDS 72-1193). For the powders calcined at 450 °C and 500 °C, a $V_2O_5$ impurity phase (JCPDS 85-0601) is detected. The powder fabricated at 450 °C is found to have 1.23 wt.% $V_2O_5$ phase. The compound calcined at 500 °C contains 97.65 wt.% $LiV_3O_8$ as the main phase with 2.35 wt.% $V_2O_5$ as the impurity phase. $V_2O_5$ has been studied widely as an insertion cathode material for lithium-ion batteries [39,40]. Recently, Cui et al. [41] synthesized a $0.8LiV_3O_8–0.2V_2O_5$ composite by a hydrothermal method, and found that the binary compound showed larger capacity and better cycling retention than the bare $LiV_3O_8$. Herein, the presence of $V_2O_5$ in $LiV_3O_8$ will have little impact on the electrochemical performance of the materials. With increasing the calcination temperature to 550 °C, 2.87 wt.% $Li_{0.3}V_2O_5$ is found in the $LiV_3O_8$ composite as the impurity phase. At 600 °C, the content of $Li_{0.3}V_2O_5$ is increased to 5.08 wt.%. The presence of $Li_{0.3}V_2O_5$ in $LiV_3O_8$ has also been reported by several groups [27,32,35,42–45]. They found that the impurity phase $Li_{0.3}V_2O_5$ had only a minor influence on the properties of the materials because $Li_{0.3}V_2O_5$ phase was also an intercalation material and/or the amount was small.

**Table 1**
Refinement parameters for $LiV_3O_8$ materials.

| $LiV_3O_8$ material | *a* | *b* | *c* | *β* |
|---|---|---|---|---|
| 450 °C | 6.6391(2) | 3.5951(7) | 12.0050(1) | 107.83(2) |
| 500 °C | 6.6479(7) | 3.5956(4) | 12.0044(5) | 107.82(6) |
| 550 °C | 6.6465(2) | 3.5956(3) | 11.9979(5) | 107.79(3) |
| 600 °C | 6.6454(1) | 3.5973(1) | 12.0011(8) | 107.76(6) |

Fig. 2 shows SEM images of the $LiV_3O_8$ powders synthesized at different temperatures. It can be seen from the images that the morphologies of the products are influenced greatly by the calcination temperature. The powder calcined at 450 °C is composed of an agglomeration of small rods. The configurations of these rods are not well recognized, suggesting that they are relatively poorly crystallized (Fig. 2a and a′). The rods are approximately 300–800 nm in length and 100–300 nm in width. With increasing the calcination temperature to 500 °C, the particles are found to be well rod-shaped and grow to larger ones (Fig. 2b and b′). The length of the rods is around 200–1000 nm and the width is 200–400 nm. With further increasing the calcination temperature to 550 °C and 600 °C, the particles grow into larger $LiV_3O_8$ rods (Fig. 2c, c′, d and d′). The morphologies of the rods are uniform, and the width of the rods can be as long as 1.5 μm. The detailed structures and morphologies of the particles synthesized at different temperatures were further analyzed by TEM and HRTEM. As shown in Fig. 3a–c, the particles show rod-like morphologies, such an observation is in good agreement with the SEM results (Fig. 2). It is clearly that the sizes of the rods become larger with the increase of calcination temperature from 500 to 600 °C. Enlarged TEM and HRTEM images in Fig. 3d confirm that the rod calcined at 500 °C is well crystallized. The HRTEM image as an inset in Fig. 3d shows clear lattice fringes of a rod with a regular spacing of 0.258 nm (Fig. 3 g), corresponding to the standard value for (1 1 2) plane of monoclinic $LiV_3O_8$ phase (JCPDS 72-1193). As shown in Fig. 3e, the HRTEM image of the rod calcined at 550 °C also demonstrates the well crystalline nature of the rod with a regular spacing of 0.344 nm (Fig. 3f), which is in a good match with the (0 1 1) plane of monoclinic $LiV_3O_8$.

Fig. 4 shows CV curves of the rod-like $LiV_3O_8$ synthesized at different temperatures in order to understand the $Li^+$ intercalation/deintercalation behavior during cycling. The 1st to 4th cycles have been recorded at a scanning rate of 0.1 mV $s^{-1}$ in the potential range of 2.0–4.0 V. It can be seen that the first CV curves are

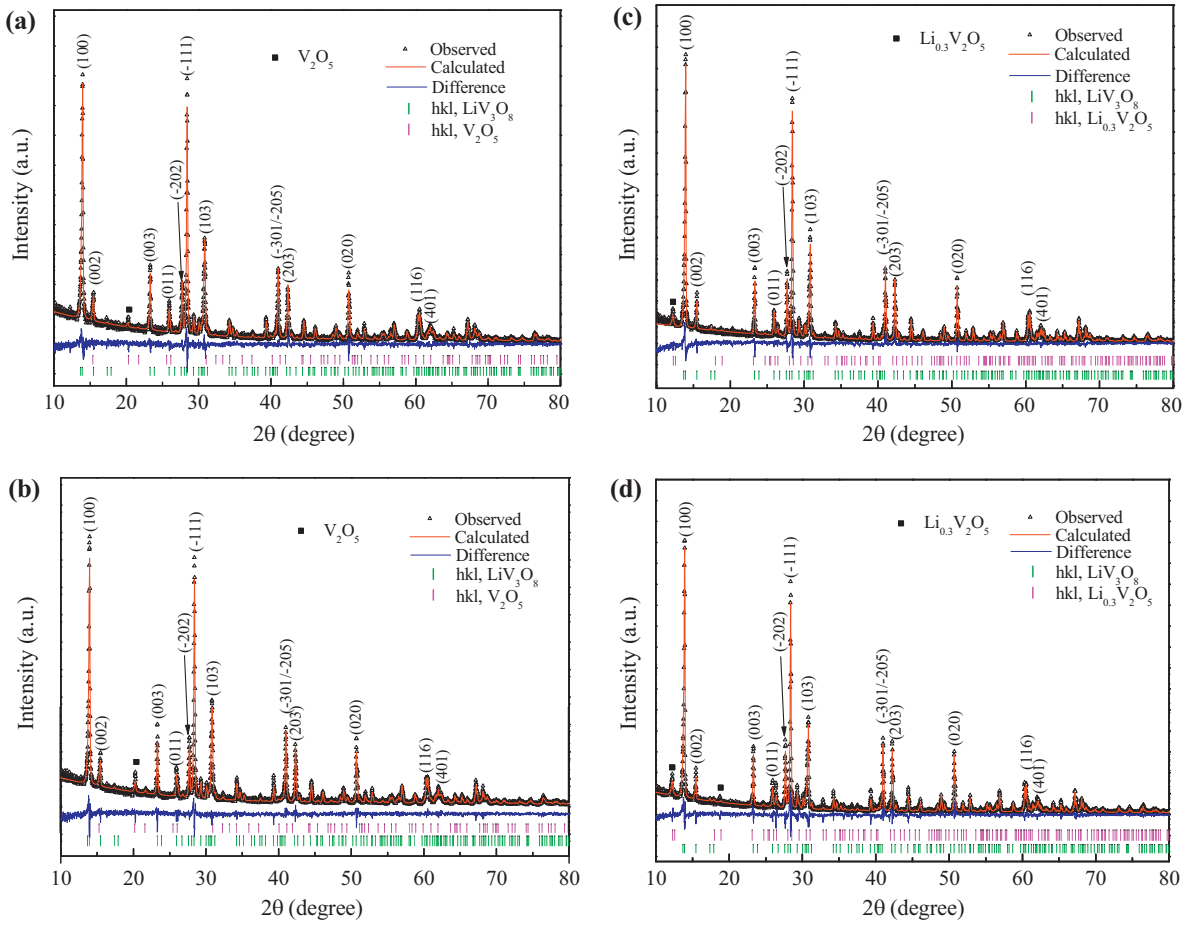


**Fig. 1.** Rietveld refinement patterns of $LiV_3O_8$ powders synthesized at (a) 450 °C, (b) 500 °C, (c) 550 °C and (d) 600 °C.

rather different from the rest, which may be ascribed to the activation of the electrodes during the first CV scan [15,33]. For the cathode materials synthesized at 450 °C and 500 °C, the features of two CV curves are similar to each other. Both the electrodes show four main oxidation peaks (near 2.42, 2.47, 2.78 and 2.84 V) and four main reduction peaks (near 2.30, 2.51, 2.72 and 2.80 V), which can be attributed to several phase transformations between the couples of $Li_{1+x}V_3O_8$ ($x = 0.1–3$) [6,15,33]. A reduction peak around 2.38 V and an oxidation/reduction peak around 3.20–3.34 V are also observed in the two electrodes, which belong to the active phase $V_2O_5$ [46,47]. In addition, the cathode material prepared at 450 °C shows broader anodic/cathodic peaks than the one synthesized at 500 °C, indicating a sluggish $Li^+$ intercalation/deintercalation process due to its low crystallinity. Whereas more highly symmetrical

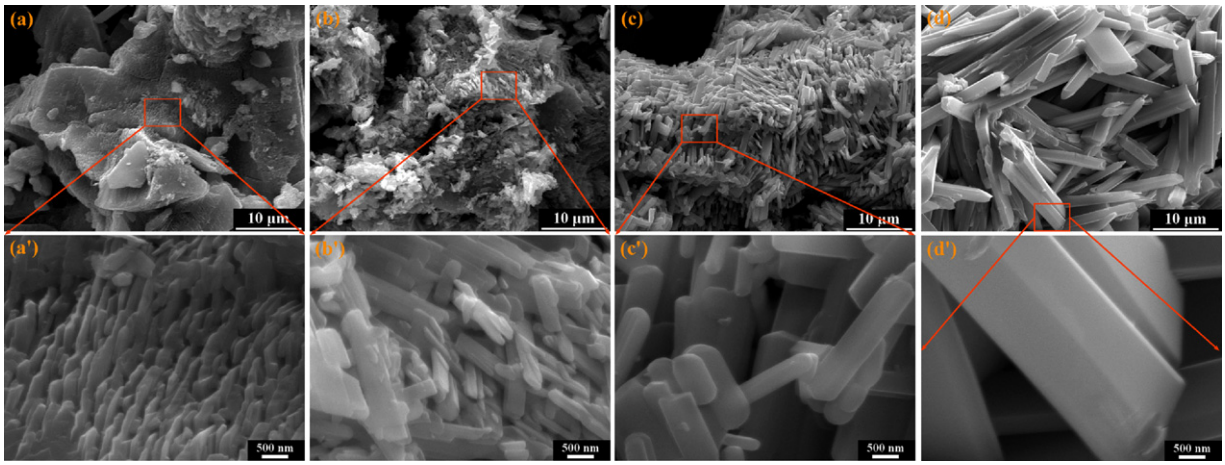


**Fig. 2.** SEM images of $LiV_3O_8$ powders: (a) 450 °C and (a′) magnified image of 450 °C; (b) 500 °C and (b′) magnified image of 500 °C; (c) 550 °C and (c′) magnified image of 550 °C; (d) 600 °C and (d′) magnified image of 600 °C.

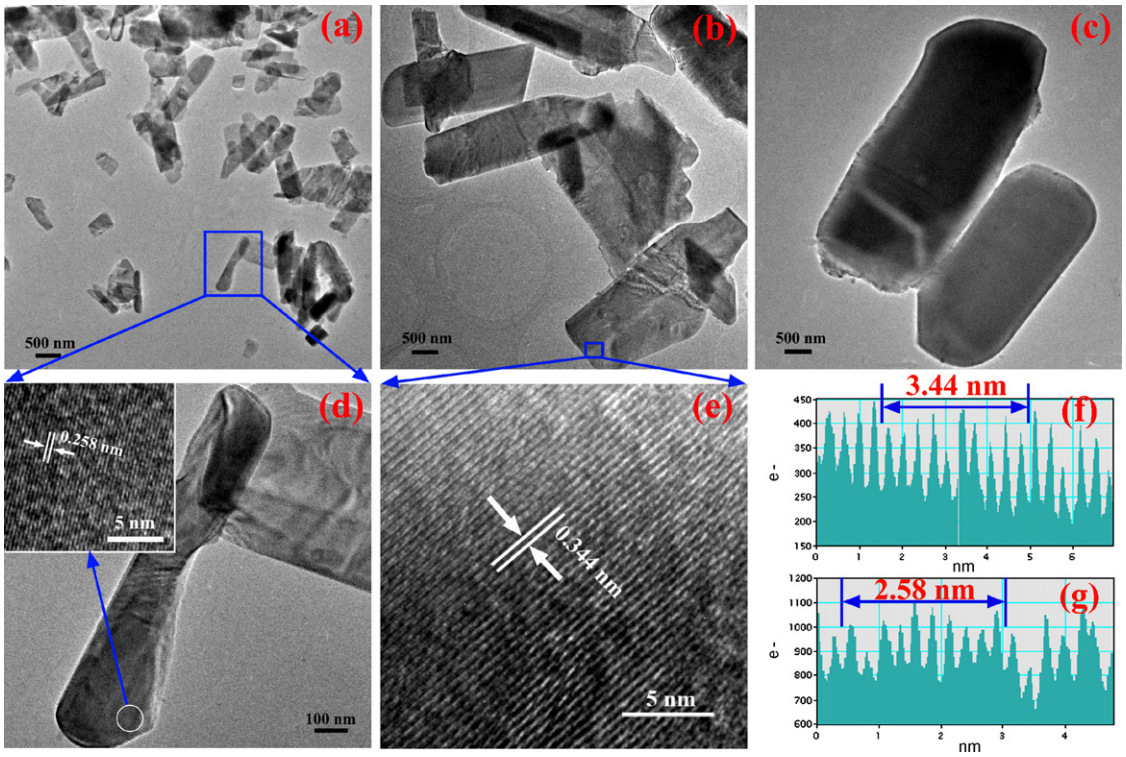


**Fig. 3.** TEM images of $LiV_3O_8$ synthesized at: (a) 500 °C, (b) 550 °C and (c) 600 °C. (d) An enlarged TEM image from (a) (indicated by a rectangular window in panel (a)). The inset is a HRTEM image corresponding to the region marked with the white circle. (e) A HRTEM image from (b) (indicated by a rectangular window in panel (b)). (f) The change of space distance from (e). (f) The change of space distance from the inset in (d).

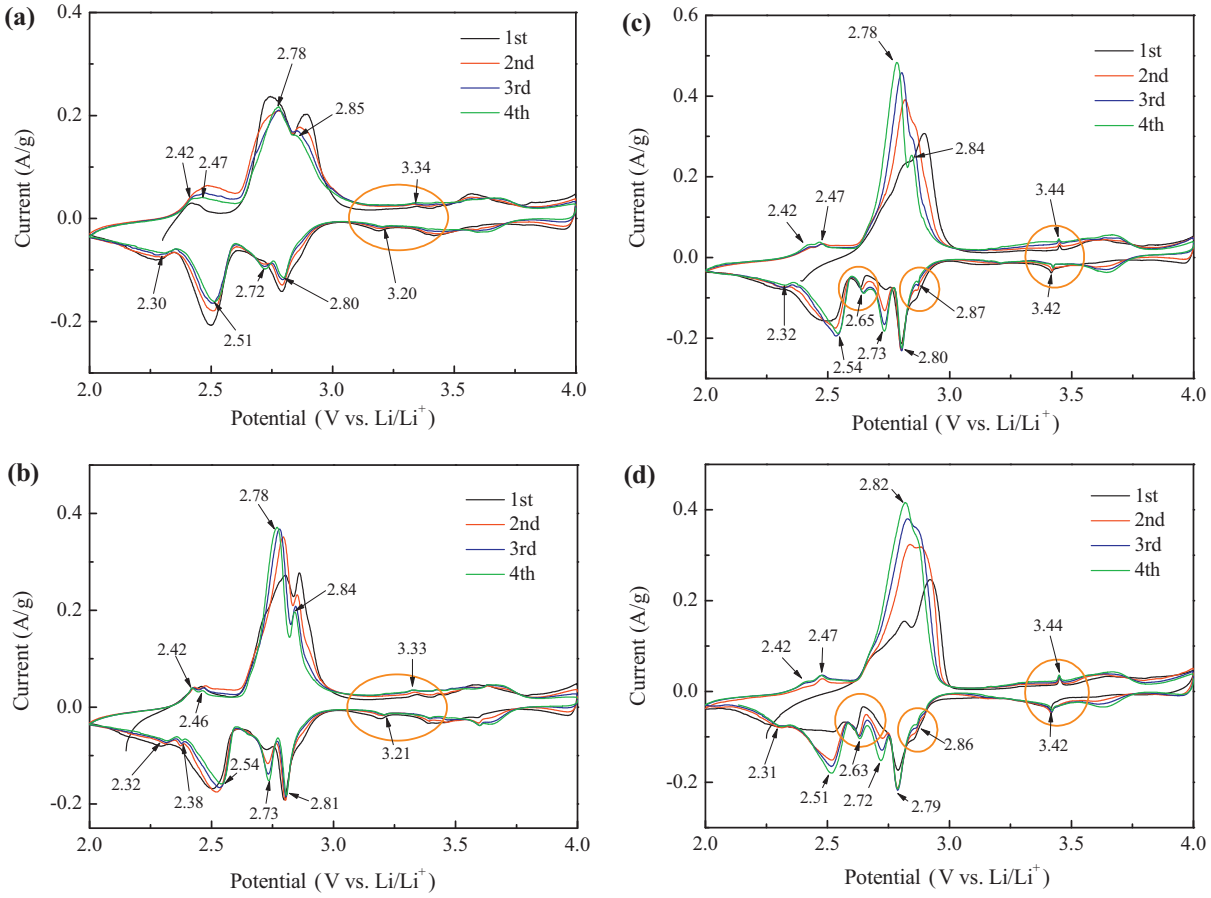


**Fig. 4.** CV curves of the $LiV_3O_8$ composites synthesized at different temperatures: (a) 450 °C, (b) 500 °C, (c) 550 °C and (d) 600 °C. Scan rate: 0.1 mV $s^{-1}$, potential range: 2.0–4.0 V.

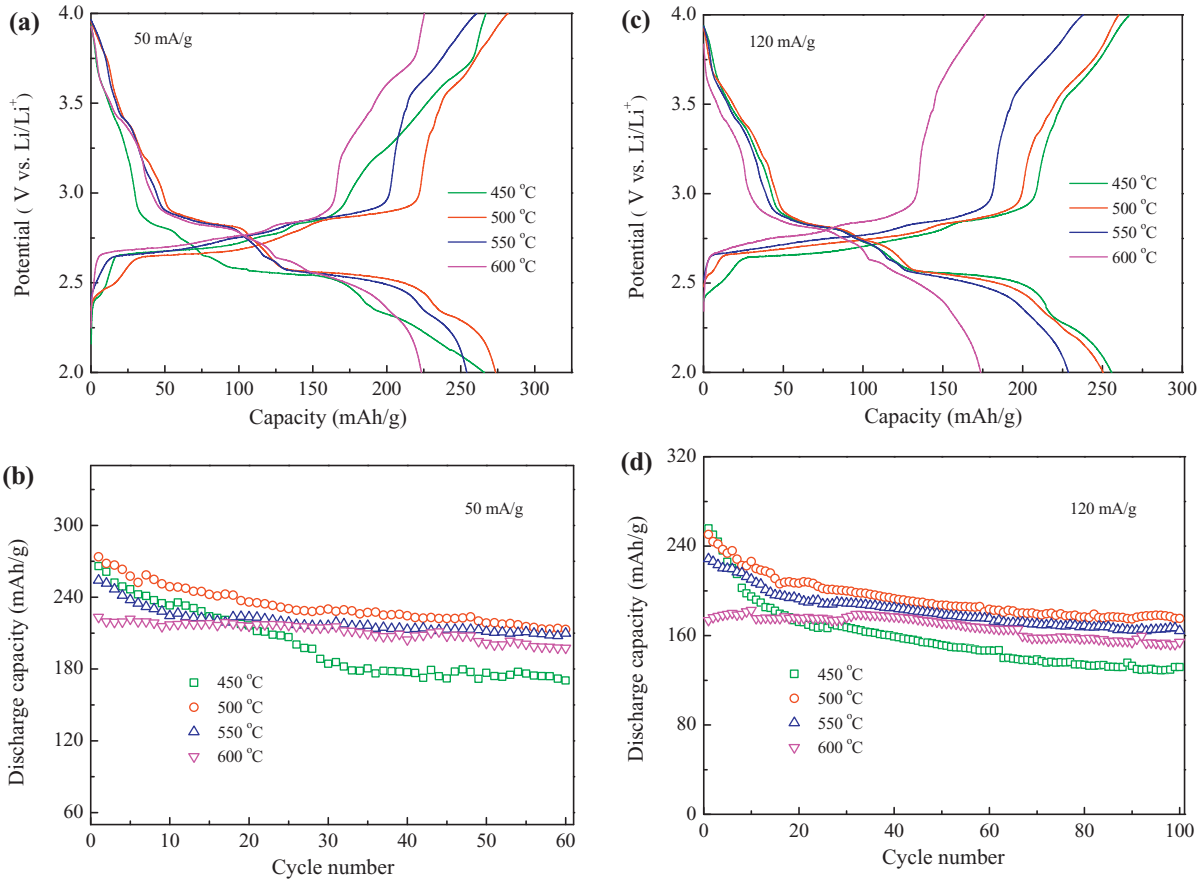


**Fig. 5.** (a) The initial charge–discharge curves and (b) cycling performance at a current density of 50 mA $g^{-1}$. (c) The initial charge-discharge curves and (d) cycling performance at a current density of 120 mA $g^{-1}$. The discharge current densities are the same as the charge current densities correspondingly.

and sharper anodic/cathodic peaks suggest excellent reversibility of the $Li^+$ extraction and insertion reactions [27,48,49]. With increasing the calcination temperature to 550 °C and 600 °C, both of the electrodes are also composed of four main oxidation peaks and four main reduction peaks, which are similar to those synthesized at 450 °C and 500 °C. The anodic peak around 3.44 V and the cathodic peaks around 2.63, 2.87 and 3.42 V are belonged to the other active phase $Li_{0.3}V_2O_5$, which are similar to those data in previous reports [27,32,35,42–45].

Fig. 5a shows the initial charge/discharge curves of $LiV_3O_8$ synthesized at different temperatures between 2.0 V and 4.0 V at a current density of 50 mA $g^{-1}$. It can be seen that all the electrodes display four main charge plateaus and four main discharge plateaus, which correspond to the CV curves as shown in Fig. 4. It is obvious that the charge/discharge curves of the cathode material synthesized at 500 °C exhibit the lowest difference between charge and discharge potential plateaus and the highest discharge potential plateau. The cathode material synthesized at 600 °C has the lowest discharge plateau, and only a discharge capacity of 223.2 mAh $g^{-1}$ can be obtained due to the large size of rods. The cathode material prepared at 500 °C delivers an initial discharge capacity of 273.6 mAh $g^{-1}$, which is higher than those synthesized at 450 °C (265.9 mAh $g^{-1}$), 550 °C (254.1 mAh $g^{-1}$) and 600 °C (223.2 mAh $g^{-1}$). After 60 cycles, it can still sustain a discharge capacity of 213 mAh $g^{-1}$, whereas only 170.4 mAh $g^{-1}$ can be achieved for the one prepared at 450 °C, as shown in Fig. 5b. Fig. 5c and d presents the initial charge–discharge curves and cycling performance at a current density of 120 mA $g^{-1}$, respectively. In Fig. 5c, the charge/discharge curves of the electrodes at a higher current density of 120 mA $g^{-1}$ are similar to those at 50 mA $g^{-1}$. The cathode material prepared at 450 °C delivers the highest initial discharge capacity of 255.8 mAh $g^{-1}$, but exhibits a poor cycling

**Table 2**
Comparison of rod-like $LiV_3O_8$ prepared by different methods.

| Synthesis method | Composition | Temperature (°C)/time (h) | Current density | Potential window (V) | Capacity (mAh $g^{-1}$) |
|---|---|---|---|---|---|
| Hydrothermal [31] | $LiV_3O_8$ | 300/12 | 0.3 mA $cm^{-2}$ | 2.0–4.0 | ~276 |
| | | | | 1.8–4.0 | 302 |
| Surfactant-assisted polymer precursor method [32] | $LiV_3O_8$ | 550/2 | 120 mA $g^{-1}$ | 2.0–4.0 | 191 |
| From $VO_2$ nanorods [33] | $LiV_3O_8$ | 450/10 | 100 mA $g^{-1}$ | 1.5–4.5 | ~249 |
| | | | | 2.0–4.0 | ~210 |
| Thermal co-decomposition method [35] | $(1-x)LiV_3O_8{\cdot}xLi_{0.3}V_2O_5$ | 350/10 | 100 mA $g^{-1}$ | 1.5–4.0 | 320 |
| | | | | 2.0–4.0 | ~275 |
| This work | $(1-x)LiV_3O_8{\cdot}xV_2O_5$ | 500/6 | 120 mA $g^{-1}$ | 2.0–4.0 | 250.4 |

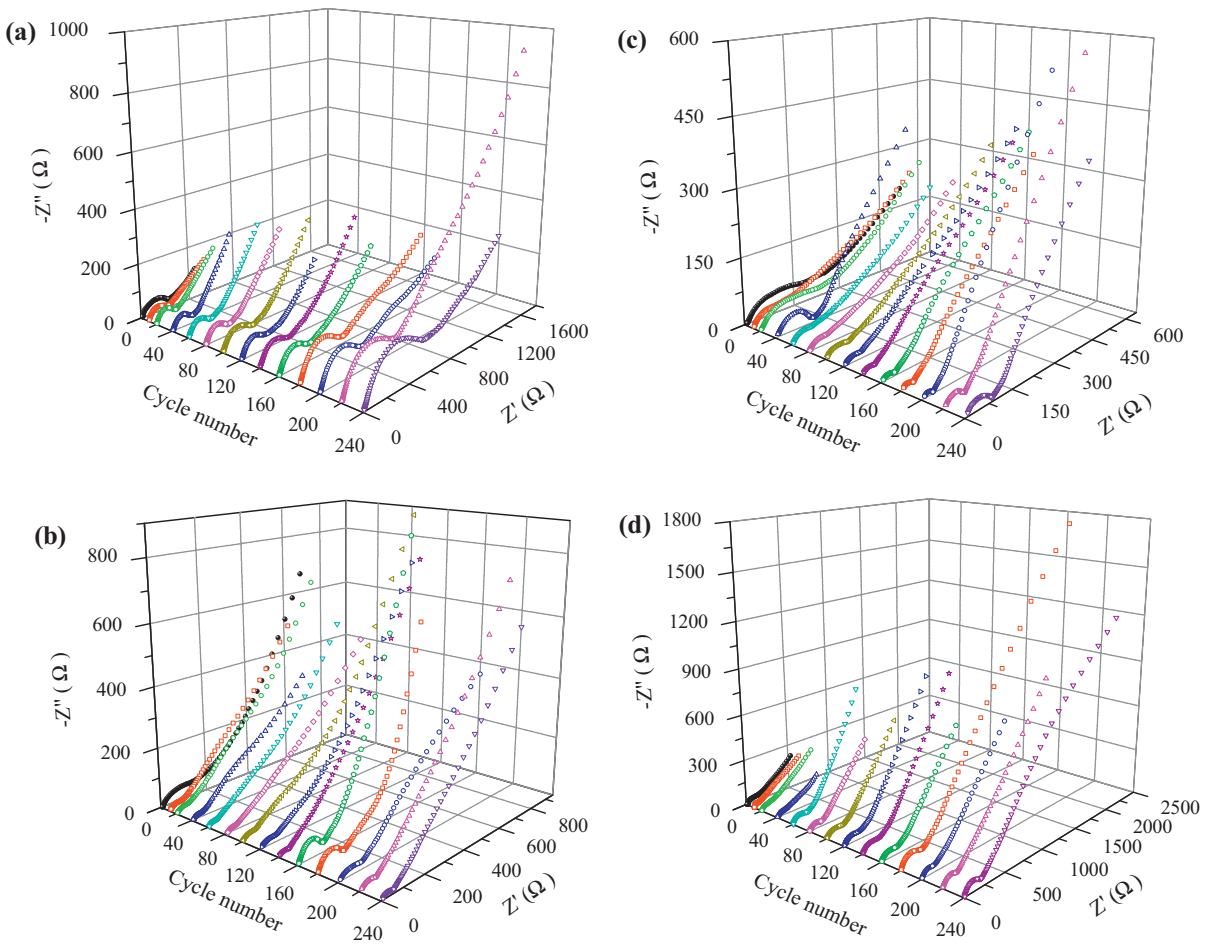


**Fig. 6.** Three-dimensional Nyquist plots measured after different number of cycles (around 2.60 V after each cycle: (a) 450 °C, (b) 500 °C, (c) 550 °C and (d) 600 °C.

ability, and only 131.7 mAh $g^{-1}$ can be obtained after 100 cycles. The poor cycling performance can be mainly attributed to the low crystallinity of the compound. For the rod-like material synthesized at 500 °C, an initial discharge capacity of 250.4 mAh $g^{-1}$ can be obtained and shows good cycling performance at a high current density of 120 mA $g^{-1}$ (Fig. 5d). The discharge capacity of our $LiV_3O_8$ rods exceeds some of the previously reported $LiV_3O_8$, and is also comparable to some results of the $LiV_3O_8$ rods in the same potential window at a current density around 120 mA $g^{-1}$, as shown in Table 2. It is well known that one-dimensional rods possess distinct advantages such as fast electron transport and ion diffusion, large surface-to-volume ratio and facile strain relaxation during charge and discharge process [28–30]. These outstanding features are favorable for achieving good electrochemical properties. In this work, the rod-like $LiV_3O_8$ synthesized by a novel method exhibits good lithium storage performance, indicating that the resulting rods are promising cathode materials for lithium-ion batteries.

Fig. 6 shows the three-dimensional Nyquist plots of the $LiV_3O_8$ electrodes after different number of cycles (around 2.60 V after each cycle). The EIS were recorded at room temperature during 1st to 240th discharge–charge cycles. It can be found that all of the plots are mainly composed of a small intercept at high frequency, a semicircle at high to medium frequency and a linear part in the low frequency. The impedance spectra are fitted using the equivalent circuit model of Fig. 7. The small intercept is almost the same for the electrodes at about 5–12 Ω, which corresponds to the solution resistance of the cell ($R_{el}$). $R_{sl}$ and $C_{sl}$ stand for the $Li^+$ migration resistance and capacity of surface layer, respectively; $R_{ct}$ and $C_{dl}$ stand for the related charge-transfer resistance and double-layer capacitance, respectively; $Z_W$ represents the diffusion-controlled Warburg impedance in the low frequency [50–54]. The fitting results of $R_{sl}$ and $R_{ct}$ according to the equivalent circuit are presented in Fig. 8a and b, respectively. It is clearly that $R_{sl}$ and $R_{ct}$ of the electrode obtained at 450 °C are obviously higher than those synthesized in the temperature range of 500–600 °C, indicating the high polarization of the electrode. The values of $R_{ct}$ for the electrode obtained at 450 °C increase significantly with prolonging the cycle number as shown in Fig. 8b. For the electrode obtained at 500 °C, the value of $R_{ct}$ is 108.1 Ω in the first cycle, but decreases to 31.5 Ω after 10 cycles. Even after 240 cycles, the value of $R_{ct}$ is still kept around 30 Ω, suggesting low polarization. Thus, the rod-like cathode material synthesized at 500 °C shows a good cycling behavior.

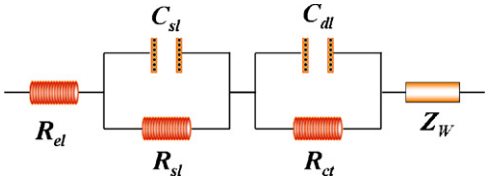


**Fig. 7.** Equivalent circuit model for $LiV_3O_8$ electrodes.

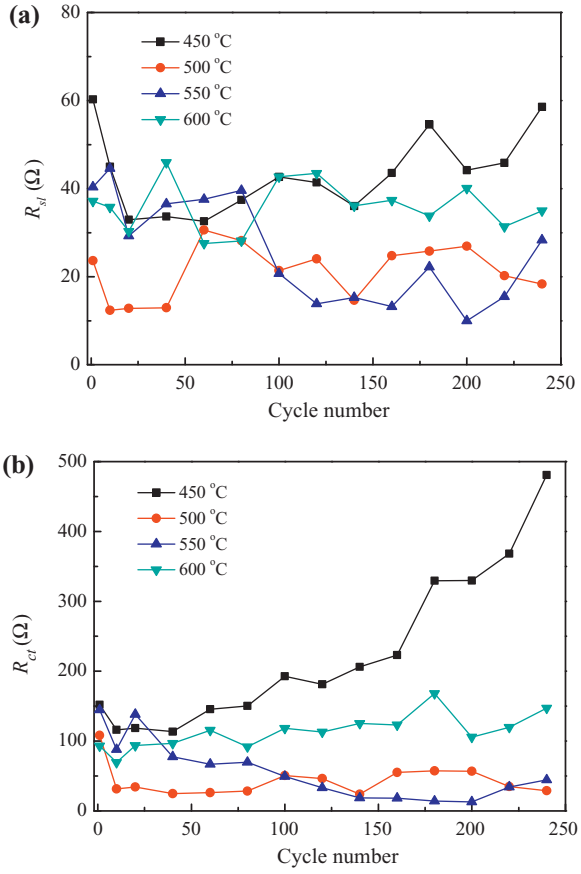


**Fig. 8.** Variation of (a) $R_{sf}$ and (b) $R_{ct}$ with cycle number calculated from fitting the Nyquist plots.

## 4. Conclusions

$LiV_3O_8$ rods were successfully prepared by using carbamide-assisted rheological phase reaction method. Electrochemical performance measurements indicate that the rod-like cathode material synthesized at 500 °C shows a high discharge capacity of 273.6 mAh $g^{-1}$ between 2.0 V and 4.0 V at a current density of 50 mA $g^{-1}$, and good cyclability. The excellent electrochemical performance of the as-synthesized electrode can be attributed to the one-dimensional structure, which favors electron transport and ion diffusion, and relieves strain relaxation during charge–discharge cycling. Based on above experimental results, the rod-like $LiV_3O_8$ would be of potential candidate for rechargeable lithium batteries.

## References

[1] X.L. Ji, K.T. Lee, L.F. Nazar, Nat. Mater. 8 (2009) 500.
[2] Y. Wang, G.Z. Cao, Adv. Mater. 20 (2008) 2251.
[3] S. Panero, M. Pasquali, G. Pistoia, J. Electrochem. Soc. 130 (1983) 1225.
[4] J. Kawakita, T. Miura, T. Kishi, J. Power Sources 83 (1999) 79.
[5] M. Dubarry, J. Gaubicher, D. Guyomard, O. Durupthy, N. Steunou, J. Livage, N. Dupré, C.P. Grey, Chem. Mater. 17 (2005) 2276.
[6] L. Liu, L.F. Jiao, J.L. Sun, Y.H. Zhang, M. Zhao, H.T. Yuan, Y.M. Wang, Electrochim. Acta 53 (2008) 7321.
[7] J.G. Xie, J. Xiao, H. Zhan, Y.H. Zhou, Chin. J. Chem. 21 (2003) 232.
[8] P. Rozier, M. Morcrette, P. Martin, L. Laffont, J-M. Tarascon, Chem. Mater. 17 (2005) 984.
[9] J.L. Sun, L.F. Jiao, H.T. Yuan, L. Liu, X. Wei, Y.L. Miao, L. Yang, Y.M. Wang, J. Alloys Compd. 472 (2009) 363.
[10] S.V. Pouchko, A.K. Ivanov-Schitz, T.L. Kulova, A.M. Skundin, E.P. Turevskaya, Solid State Ionics 151 (2002) 129.
[11] C.Q. Feng, L.F. Huang, Z.P. Guo, J.Z. Wang, H.K. Liu, J. Power Sources 174 (2007) 548.
[12] M. Zhao, L.F. Jiao, H.T. Yuan, Y. Feng, M. Zhang, Solid State Ionics 178 (2007) 387.
[13] Y. Feng, Y.L. Li, F. Hou, J. Power Sources 187 (2009) 224.
[14] Y.M. Liu, X.C. Zhou, Y.L. Guo, Electrochim. Acta 54 (2009) 3184.
[15] L.F. Jiao, L. Liu, J.L. Sun, L. Yang, Y.H. Zhang, H.T. Yuan, Y.M. Wang, X.D. Zhou, J. Phys. Chem. C 112 (2008) 18249.
[16] N.H. Idris, M.M. Rahman, J.-Z. Wang, Z.-X. Chen, H.-K. Liu, Compos. Sci. Technol. 71 (2011) 343.
[17] C.Q. Feng, S.Y. Chew, Z.P. Guo, J.Z. Wang, H.K. Liu, J. Power Sources 174 (2007) 1095.
[18] S.Y. Chew, J. Sun, J. Wang, H. Liu, M. Forsyth, D.R. MacFarlane, Electrochim. Acta 53 (2008) 6460.
[19] S.Y. Chew, C. Feng, S.H. Ng, J. Wang, Z. Guo, H. Liu, J. Electrochem. Soc. 154 (2007) A633.
[20] A. Yu, N. Kumagai, Z. Liu, J.Y. Lee, J. Power Sources 74 (1998) 117.
[21] J.J. Feng, X.Z. Liu, X.M. Zhang, J.Z. Jiang, J. Zhao, M. Wang, J. Electrochem. Soc. 156 (2009) A768.
[22] L. Liu, L.F. Jiao, J.L. Sun, Y.H. Zhang, M. Zhao, H.T. Yuan, Y.M. Wang, J. Alloys Compd. 471 (2009) 352.
[23] H. Yang, J. Li, X.-G. Zhang, Y.-L. Jin, J. Mater. Process. Technol. 207 (2008) 265.
[24] S.H. Ju, Y.C. Kang, Electrochim. Acta 55 (2010) 6088.
[25] H.M. Liu, Y.G. Wang, W.S. Yang, H.S. Zhou, Electrochim. Acta 56 (2011) 1392.
[26] H. Ma, Z.Q. Yuan, F.Y. Cheng, J. Liang, Z.L. Tao, J. Chen, J. Alloys Compd. 509 (2011) 6030.
[27] H.-L. Zhang, J.R. Neilson, D.E. Morse, J. Phys. Chem. C 114 (2010) 19550.
[28] Y.Q. Song, S.S. Qin, Y.W. Zhang, W.Q. Gao, J.P. Liu, J. Phys. Chem. C 114 (2010) 21158.
[29] Y. Yang, C. Xie, R. Ruffo, H. Peng, D.K. Kim, Y. Cui, Nano Lett. 9 (2009) 4109.
[30] H.W. Liu, C.X. Cheng, X.T. Huang, J.L. Li, Electrochim. Acta 55 (2010) 8461.
[31] H.Y. Xu, H. Wang, Z.Q. Song, Y.W. Wang, H. Yan, M. Yoshimura, Electrochim. Acta 49 (2004) 349.
[32] A. Sakunthala, M.V. Reddy, S. Selvasekarapandian, B.V.R. Chowdari, P.C. Selvin, J. Phys. Chem. C 114 (2010) 8099.
[33] H.M. Liu, Y.G. Wang, K.X. Wang, Y.R. Wang, H.S. Zhou, J. Power Sources 192 (2009) 668.
[34] A. Caballero, J. Morales, O.A. Vargas, J. Power Sources 195 (2010) 4318.
[35] A.Q. Pan, J. Liu, J.G. Zhang, G.Z. Cao, W. Xu, Z.M. Nie, X. Jie, D. Choi, B.W. Arey, C.M. Wang, S.Q. Liang, J. Mater. Chem. 21 (2011) 1153.
[36] L. Lutterotti, S. Gialanella, Acta Mater. 46 (1998) 101.
[37] L. Lutterotti, S. Matthies, H.-R. Wenk, J. Appl. Phys. 81 (1997) 594.
[38] J.T. Han, Y.H. Huang, W. Huang, J.B. Goodenough, J. Am. Chem. Soc. 128 (2006) 14454.
[39] A.-M. Cao, J.-S. Hu, H.-P. Liang, L.-J. Wan, Angew. Chem. Int. Ed. 44 (2005) 4391.
[40] K.-I. Park, H.-M. Song, Y. Kim, S. Mho, W.I. Cho, I.-H. Yeo, Electrochim. Acta 55 (2010) 8023.
[41] P. Cui, Z.J. Jia, L.Y. Li, T. He, Electrochim. Acta 56 (2011) 4571.
[42] T.J. Patey, S.H. Ng, R. Büchel, N. Tran, F. Krumeich, J. Wang, H.K. Liu, P. Novák, Electrochem. Solid-State Lett. 11 (2008) A46.
[43] Y. Zhou, H.-F. Yue, X.-Y. Zhang, X.-Y. Deng, Solid State Ionics 179 (2008) 1763.
[44] M. Dubarry, J. Gaubicher, P. Moreau, D. Guyomard, J. Electrochem. Soc. 153 (2006) A259.
[45] N. Tran, K.G. Bramnik, H. Hibst, J. Prölß, N. Mronga, M. Holzapfel, W. Scheifele, P. Novák, J. Electrochem. Soc. 155 (2008) A384.
[46] A. Sakunthala, M.V. Reddy, S. Selvasekarapandian, B.V.R. Chowdari, P. Christopher Selvin, Energy Environ. Sci. 4 (2011) 1712.
[47] Y.J. Wei, C.-W. Ryu, K.-B. Kim, J. Alloys Compd. 459 (2008) L13.
[48] Y.Q. Qiao, J.P. Tu, J.Y. Xiang, X.L. Wang, Y.J. Mai, D. Zhang, W.L. Liu, Electrochim. Acta 56 (2011) 4139.
[49] Y.Q. Qiao, J.P. Tu, X.L. Wang, D. Zhang, J.Y. Xiang, Y.J. Mai, C.D. Gu, J. Power Sources 196 (2011) 7715.
[50] K.M. Shaju, G.V. Subba Rao, B.V.R. Chowdari, Electrochim. Acta 48 (2003) 2691.
[51] J.Y. Xiang, J.P. Tu, Y.Q. Qiao, X.L. Wang, J. Zhong, D. Zhang, C.D. Gu, J. Phys. Chem. C 115 (2011) 2505.
[52] Y.Q. Qiao, J.P. Tu, Y.J. Mai, L.J. Cheng, X.L. Wang, C.D. Gu, J. Alloys Compd. 509 (2011) 7181.
[53] L. Zhang, X.L. Wang, J.Y. Xiang, Y. Zhou, S.J. Shi, J.P. Tu, J. Power Sources 195 (2010) 5057.
[54] Y.Q. Qiao, X.L. Wang, Y. Zhou, J.Y. Xiang, D. Zhang, S.J. Shi, J.P. Tu, Electrochim. Acta 56 (2010) 510.